ELSEVIER

Journal of Alloys and Compounds 300–301 (2000) 123–130

Journal of ALLOYS AND COMPOUNDS

www.elsevier.com/locate/jallcom

Yb^{3+}–Er^{3+}-codoped $LaLiP_4O_{12}$ glass: a new eye-safe laser at 1535 nm

A.-F. Obaton[a,c], C. Parent[b], G. Le Flem[b], P. Thony[d], A. Brenier[c], G. Boulon[c,*]

[a]*LEMMA, Université de La Rochelle, 17042 La Rochelle Cedex 01, France*
[b]*ICMCB, Université Bordeaux I, UPR 9048 CNRS, 33608 Pessac Cedex, France*
[c]*LPCML, Université Claude Bernard Lyon 1, UMR CNRS 5620, 69622 Villeurbanne Cedex, France*
[d]*LETI-CEA-CENG,38054 Grenoble Cedex 9, France*

Abstract

The main spectroscopic and thermal properties of Yb^{3+}–Er^{3+}-codoped $LaLiP_4O_{12}$ phosphate glasses show that they are very well adapted for use as eye-safe laser materials as a result of a comparison with different Yb^{3+}–Er^{3+}-codoped phosphate glasses.

Keywords: Phosphate glasses; Luminescence; Eye-safe lasers; Ytterbium; Erbium

1. Introduction

The main objective of this research work is to improve the optical approach of the Er^{3+} ion emission for eye-safe laser sources near 1540 nm. Today, the industrial phosphate glasses provide the best performances among all crystals and glasses, although the low thermal conductivity of glasses remains problematic. Therefore, better knowledge of optical and thermal properties of phosphate glasses is needed. As a matter of fact, we have chosen to synthesize various compositions of Yb^{3+}–Er^{3+}-codoped phosphate vitreous matrices in order to compare their properties.

Er^{3+}emission transition occurs within this wavelength range corresponding to the $^4I_{13/2}\rightarrow{}^4I_{15/2}$ transition. However, Er^{3+} absorption itself is too weak to allow direct pumping and so, energy transfers are required. The most efficient ones are given by Yb^{3+} ions under absorption from the $^2F_{7/2}\rightarrow{}^2F_{5/2}$ transition, followed by energy transfer to the $^4I_{11/2}$ Er^{3+} level and fast nonradiative transition to the Er^{3+} $^4I_{13/2}$ level which emits the expected fluorescence (Fig. 1). As a matter of fact, Yb^{3+} concentration has to be optimized to get the highest absorption coefficient. Although comparative analyses have been previously published [1–3], we especially would like to show in this paper, additional results and to point out that Yb^{3+}–Er^{3+}-codoped $LaLiP_4O_{12}$ glass is an excellent laser material, compared with commercialized ones.

2. Experimental

2.1. Synthesis process

The basis compositions of the investigated glasses are: $75.5P_2O_5$–$10.5Li_2O$–$(14-x-y)$ La_2O_3-x Yb_2O_3-y Er_2O_3 (mol%). In the following text, the samples are called Yb^{3+}–Er^{3+}-codoped $LaLiP_4O_{12}$ glasses. The phosphate glasses were prepared from mixtures of $NH_4H_2PO_4$ (Merk 99%), Li_2CO_3 (Merk 99.997%), La_2O_3 (Prolabo 99.995%), Yb_2O_3 (Aldrich 99.99%) and Er_2O_3 (Aldrich 99.99%). The elaboration processes have been previously reported [4]. The batch mixture is introduced in a vitreous carbon crucible and preheated at 200°C for 3 h to decompose and melt the dihydrogenammonium phosphate. After additional heating for 15 h at 550°C, the temperature is raised up to the melting point, 1350°C under a stream of argon to preserve the crucible and maintained for 1 h. The melt is rapidly poured onto a preheated graphite mould. Finally, glasses are annealed 20°C below the glass transition temperature determined by thermodifferential analysis at 450°C and then cooled down to room temperature at

*Corresponding author. Tel.: +33-4-7244-8271; fax: +33-4-7243-1130.
E-mail address: boulon@pcml.univ-lyon1.fr (G. Boulon)

0925-8388/00/$ – see front matter
PII: S0925-8388(99)00742-2

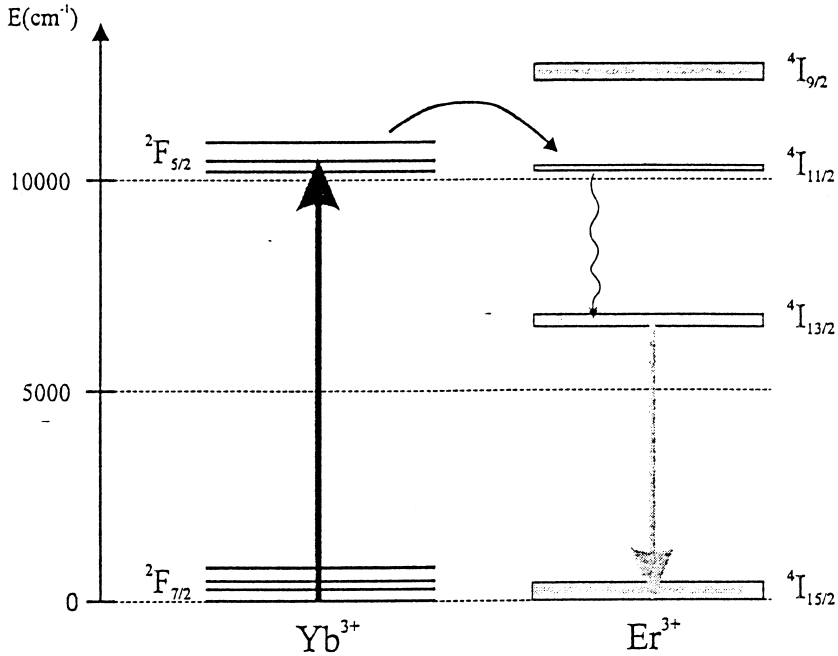

Fig. 1. Energy transfer scheme between Yb^{3+} and Er^{3+} ions for eye-safe laser purpose near 1540 nm.

30°C/h. The proportions of the starting materials are chosen carefully to take account of the P_2O_5 losses which occur by evaporation during the elaboration process.

The $LaLiP_4O_{12}$ glass synthesis process is then well finalised. Indeed this material has been extensively studied as a potential microlaser source due to a low self-concentration quenching of Nd^{3+} neodymium emission but optical properties of Yb^{3+}–Er^{3+} codopants have not yet been reported before. Spectroscopic and thermal properties have been compared with those of several other codoped glassy compositions such as:

- $ZnO–Al_2O_3–La_2O_3–P_2O_5$ (ZALP) (1) for its high chemical stability,
- $Al_2O_3–Li_2O–P_2O_5$– (AlLiP) for its simplicity and chemically stability,
- $NaPO_3–BaF_2–YF_3$ (NBY) fluorophosphate different from other samples by Fluor presence, which is very stable and able to accept a high amount of rare earth ions,
- Commercialized QE20 KIGRE glasses whose compositions are not revealed by the manufacturer.

3. Results

3.1. Spectroscopic analysis

3.1.1. Absorption spectra

Normalized absorption spectra of Yb^{3+}-doped phosphate glasses show similar structures at low temperature (10 K) as can be seen in Fig. 2. The $2F_{7/2}\rightarrow 2F_{5/2}$ zero-phonon line is clearly recognized at 974.6 nm. With the exception of fluorophosphate, more than three stark levels are observed for the $2F_{5/2}$ excited level for most of them. It means that deeper resolution is needed to know the accurate positions of such sublevels in order to separate vibronic and electronic spectra. Another possibility is to get at least two kinds of Yb^{3+} nonequivalent centers in pure phosphate networks, as an example La^{3+} and Li+ ion chemical environments in $LaLiP_4O_{12}$ glass. If we retain the highest intensity components, the excited-state levels correspond to the zero-line at 974.6 nm (10 260 cm^{-1}), and two stark levels at 954 nm (10 482 cm^{-1}) and 918.03 nm (10 892 cm^{-1}) respectively. Fig. 3 shows the room temperature absorption spectrum which is still resolved. The zero-line maximum is slightly moved to 977 nm as expected, and in addition, the absorption transition from the second stark level of the ground state can be seen at 1002 nm allowing its approximate energy position at 255 cm^{-1} above the ground state reference to be known. Therefore, the best wavelength to pump this glass at usual room temperature is therefore located at 977 nm (10 235 cm^{-1}). The absorption cross-section corresponding to this wavelength is 1.33×10^{-20} cm^2 which is the highest value obtained for phosphate glasses.

3.1.2. Er^{3+} emission data

The maximum of the Er^{3+} $^4I_{13/2}\rightarrow{}^4I_{15/2}$ resonant transition is found at 1535 nm at room temperature with a large bandwidth of around 21 nm (Fig. 4). The stimulated emission cross-section value of 1534 nm is 0.80×10^{-20} cm^2. This is the highest value for phosphate glasses with AlLiP and Kigre samples.

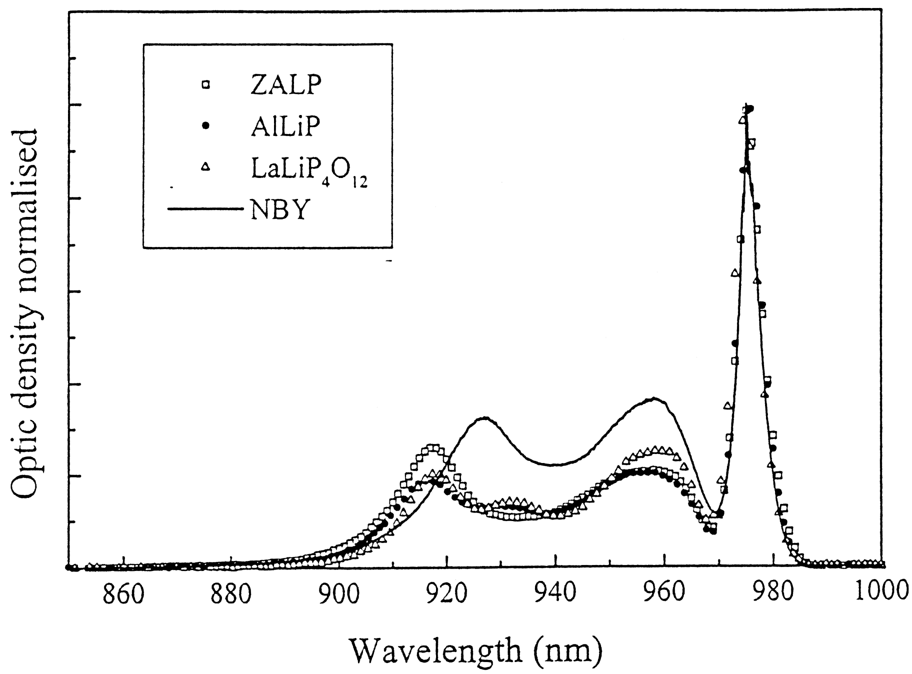

Fig. 2. Absorption spectra of Yb^{3+}-doped phosphate glasses with different compositions at low temperature (10 K).

3.1.3. Er^{3+} excited state absorption data

The excited-state absorption occurs in the range 1630–1800 nm associated with the $^4I_{13/2} \rightarrow {}^4I_{9/2}$ Er^{3+} transition whereas the emission is seen between 1440 and 1660 nm (Fig. 5). The excited-state absorption cross-section is 0.15×10^{-20} cm^2 which is about one sixth of the stimulated emission cross-section. Therefore such processes do not significantly perturb the $^4I_{13/2} \rightarrow {}^4I_{15/2}$ emission in the eye-safe range. Indeed it is a general feature of Er^{3+}-doped materials. We have also determined experimentally (exp) and mathematically (calc), the line strength $S_{exp}=7.87\times10^{-23}$ cm^2 and $S_{calc}=5.33\times10^{-23}$ cm^2 for the $^4I_{13/2} \rightarrow {}^4I_{9/2}$ transition.

Taking into account both the experimental difficulties of

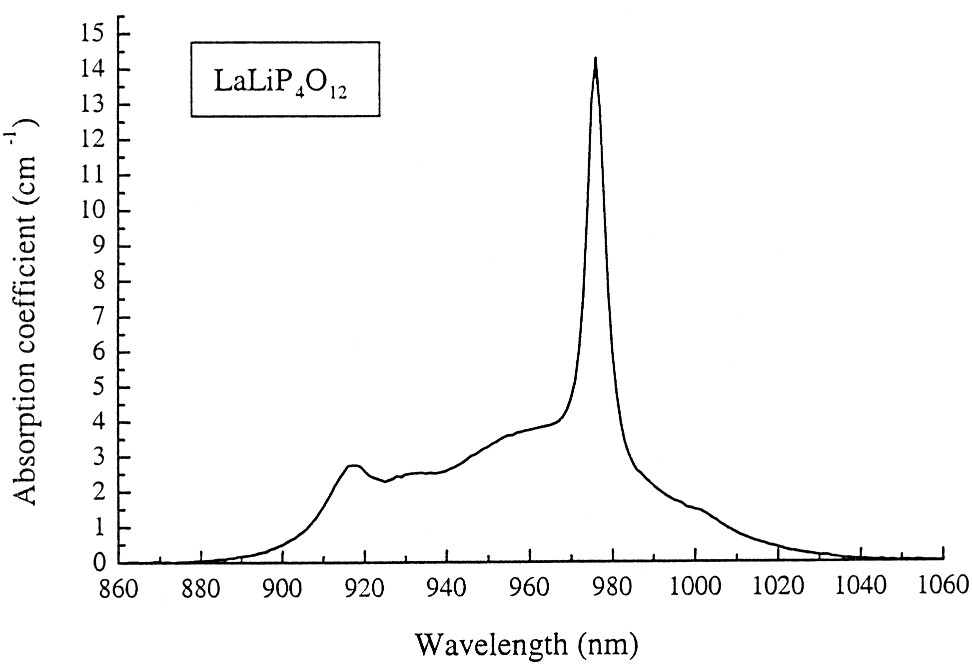

Fig. 3. Absorption spectrum Yb^{3+}-doped $LaLiP_4O_{12}$ phosphate glass at room temperature.

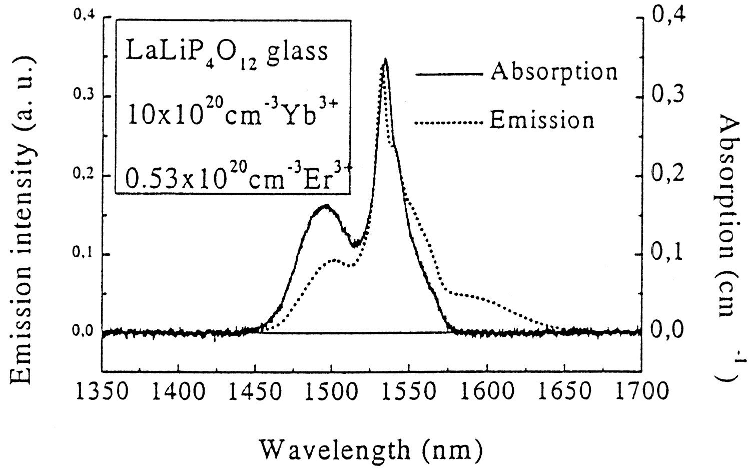

Fig. 4. Er^{3+} emission and absorption spectra in $LaLiP_4O_{12}$ phosphate glass at room temperature.

the excited state measurements and the significant approximation in the Judd–Ofelt formalism, the agreement between these two values is almost satisfactory [2].

3.1.4. Er^{3+} ion decays

The excited-state dynamics shows interesting results. As can be seen in Fig. 6, the Er^{3+} $^4I_{13/2}$ fluorescence lifetime in $LaLiP_4O_{12}$ glass has the highest values. The $^4I_{13/2}$ fluorescence lifetime (8630 μs) is very close to the radiative one (9465 μs) giving a fluorescence efficiency of η=0.91 at 1535 nm. This is the highest value of η in phosphate glasses, excepting obviously fluorophosphate glasses where radiative and fluorescence lifetimes are always close (n=0.98). On the other hand, the $^4I_{13/2}$ fluorescence rise-time is relatively short (30–40 μs), but not so short as the 20 μs of the Kigre QE20 sample.

This statement gives great importance to this type of glass. It also means that the hydroxyl group (OH^-) content which is usually responsible for the nonradiative transitions between $^4I_{11/2}$ and $^4I_{13/2}$ excited levels of Er^{3+} ions which are separated by around 3708 cm^{-1} for $LaLiP_4O_{12}$ (Fig. 1) coinciding with the vibrational energy of OH^- hydroxyl groups, is much lower in $LaLiP_4O_{12}$ than in other phosphate glasses as is clearly demonstrated in Fig. 7. It is worthwhile to especially mention the very low OH^- concentration in $LaLiP_4O_{12}$ glass, the lowest of the phosphate glasses very close to the fluorophosphate case in which there is the reaction $OH^- + F^- \rightarrow O^{2-} + HF$ drastically reducing the OH^- content. We have observed that there is an excellent agreement between fluorescence efficiencies measured from the ratio between fluorescence decays and radiative lifetimes at 1535 nm, and OH^- content in all

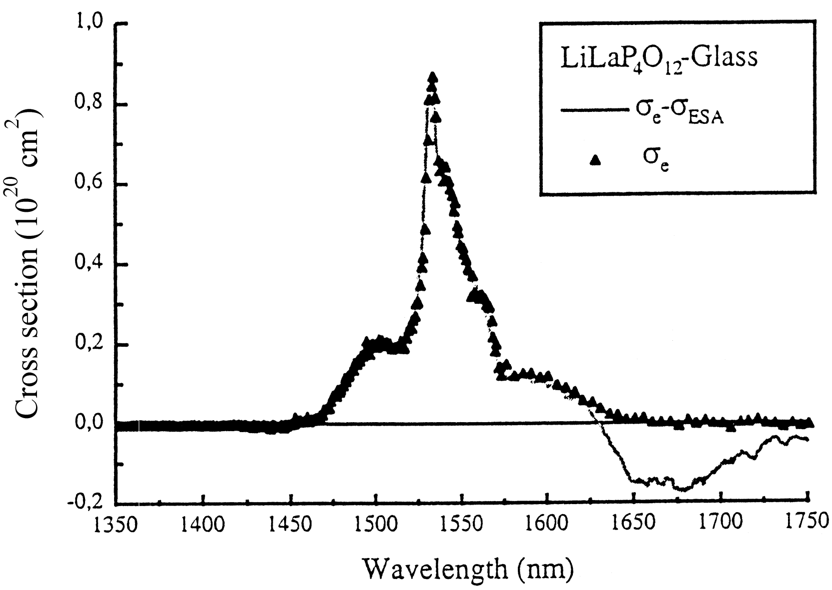

Fig. 5. Er^{3+} σ_e stimulated emission and σ_{esa} excited-state absorption cross-sections in the eye-safe range around 1535 nm.

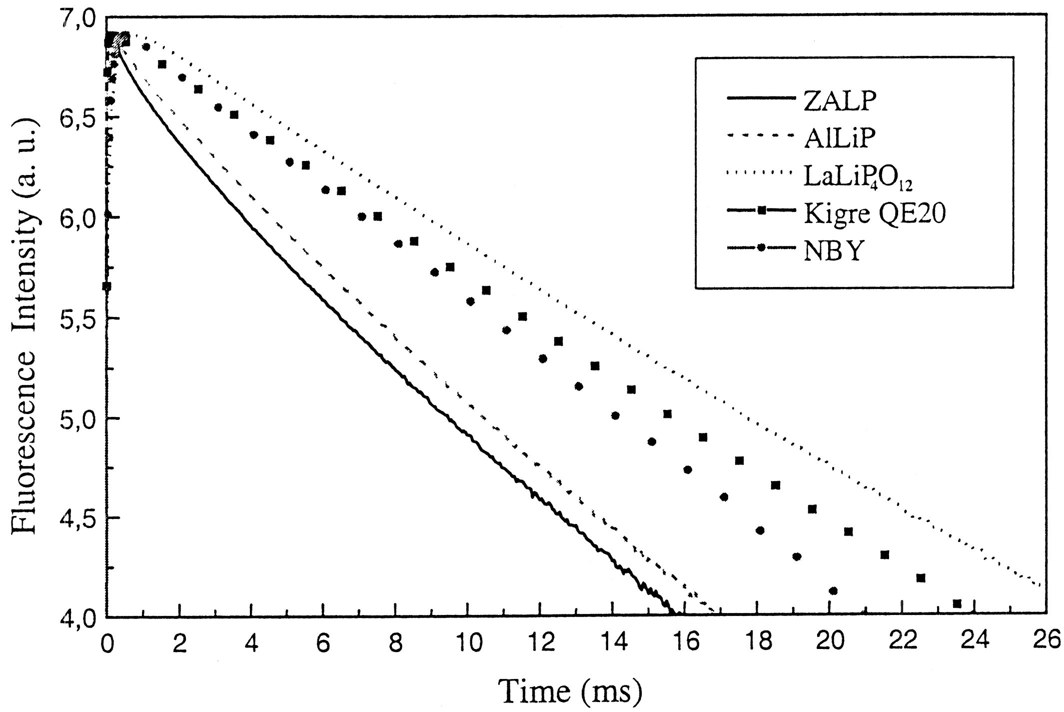

Fig. 6. Comparison of the Er^{3+} $^4I_{13/2}$ excited level fluorescence decays in different phosphate glasses.

phosphate glass samples: 0.49 ($ZnO–Al_2O_3–Al_2O_3–La_2O_3–P_2O_5$), 0.57 ($Al_2O_3–Li_2O–P_2O_5$), 0.75 (Kigre QE20), 0.91 ($LaLiP_4O_{12}$), 0.98 (fluorophosphate NBY).

3.1.5. Raman spectra

In addition to Yb^{3+} and Er^{3+} spectroscopic measurements, we have also characterized host matrices by usual Raman spectroscopy (Fig. 8). The line at 1184 cm^{-1} which has the strongest intensity in $LaLiP_4O_{12}$ is also the sharpest one and therefore we can assume that the structural disorder in this sample is lower than in the others. The strongest line and its shoulder at the slightly higher energy arises from a symmetric stretch (PO_2) and a antisymmetric stretch (PO_2) of the PO_4 unit. The band at about 700 cm^{-1} is assigned to the P–O–P stretch of quasi infinite phosphate chains. The number of phonons implied in the $^4I_{11/2}\rightarrow{}^4I_{13/2}$ Er^{3+} excited state transition is found to be equal to three for all phosphates by taking into account the 3708 cm^{-1} energy gap between levels and the 1200 cm^{-1} value of the vibrational energy. Under these conditions, we can assume that nonradiative transition probability between these two excited states is more probable than the radiative one. Indeed, we did not find any detectable emission around 2.7 μm.

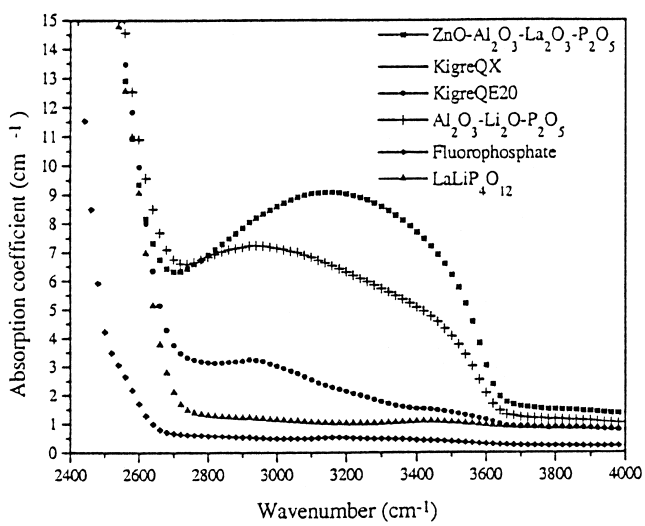

Fig. 7. Comparative analysis of OH^- absorption spectra intensity in different phosphate glasses.

Another low frequency Raman spectroscopy technique is applied to phosphate glasses in order to analyse the vibrational dynamics and the structure of glasses. The presence of a boson peak at around 50 cm^{-1} shows that the network seems not continuous but composed of short range order or so-called cohesive domains having a nanometer scale study of which is in progress [4].

3.2. Thermal properties

It is very well known that the main problem of glasses compared to crystals is their low thermal conductivity. An higher thermal conductivity (9.68×10^{-3} W cm^{-1} K^{-1}) is found for $LaLiP_4O_{12}$ compared to commercialised Kigre samples (4.88×10^{-3} W cm^{-1} K^{-1}), that is to say twice that which we may consider as a reference. This observation adds another argument in favour of this new laser

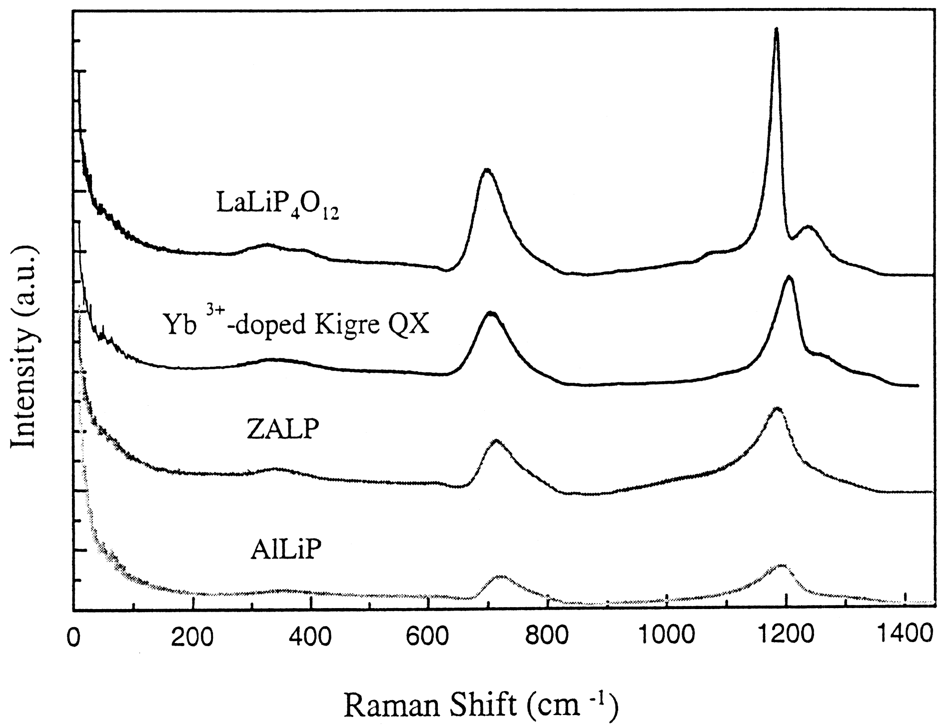

Fig. 8. Raman spectra between 100 and 1400 cm^{-1} in different phosphate glasses.

material. It is another experimental observation which makes sense in view of the highest structural order degree in $LiLaP_4O_{12}$.

3.3. Laser properties

It is well known that the Er^{3+} laser-ion energy level structure corresponds to a quasi-three levels scheme, the final state of the laser transition being a sub-level of the $^4I_{15/2}$ ground state. The main consequence is then to get reabsorption of the laser emission by resonant transitions. Such a phenomenom occurs when absorption and emission overlapping is important, which is the case in the shortest wavelength's side, as can be seen in Fig. 4. To know the gain is therefore one priority in these laser materials. By laser emission reabsorption from both, the ground state and the excited state and, on the other hand, by taking account of the excited state absorption of the pumping energy, the gain $g()$ can be associated with cross-sections as following:

$$g(\lambda) = [\sigma_e(\lambda) - \sigma_{aee}(\lambda)]N_e - \sigma_a(\lambda)N_f$$

where: σ_e (λ) is the stimulated emission cross-section, σ_{aee} (λ) is the excited state absorption cross-section and $\sigma_a(\lambda)$ is the absorption cross-section from the ground state. N_e and N_f are the higher and lower levels populations, respectively, of the laser transition.

However it has been shown that σ_{aee} (λ) excited-state absorption from $^4I_{13/2}$ can be neglected for wavelengths lower than 1600 nm. As a consequence, the previous equation can be rewritten:

$$g(\lambda) = \sigma_e(\lambda)N_e - \sigma_a(\lambda)N_f$$

The gain cross-section can be expressed from the β inversion population ratio as:

$$\sigma_g(\lambda) = \beta\sigma_e(\lambda) - (1 - \beta)\sigma_a(\lambda)$$

with

$$\beta = N_e/N_e + N_f$$

The β_{min} population threshold in order to get the laser threshold is now given by:

$$\beta_{min} = \sigma_a/\sigma_a + \sigma_e$$

The $\sigma_g(\lambda)$ gain cross-section has been deduced from absorption and emission cross-sections and reported in Fig. 9 as a function of the β inversion ratio. These spectra have the same profile whatever the nature of the Yb^{3+}–Er^{3+}–codoped glasses. We can see that in the absence of any loss inside the laser cavity, laser emission is possible for wavelengths within the spectral range 1475–1600 nm. We were also able to check that in the eye-safe range, between 1530 nm and 1570 nm, the population inversion ratio needed is around 30–50%.

The laser tests have been done in the LETI–CEA laboratory at Grenoble under laser-diode pumping of the

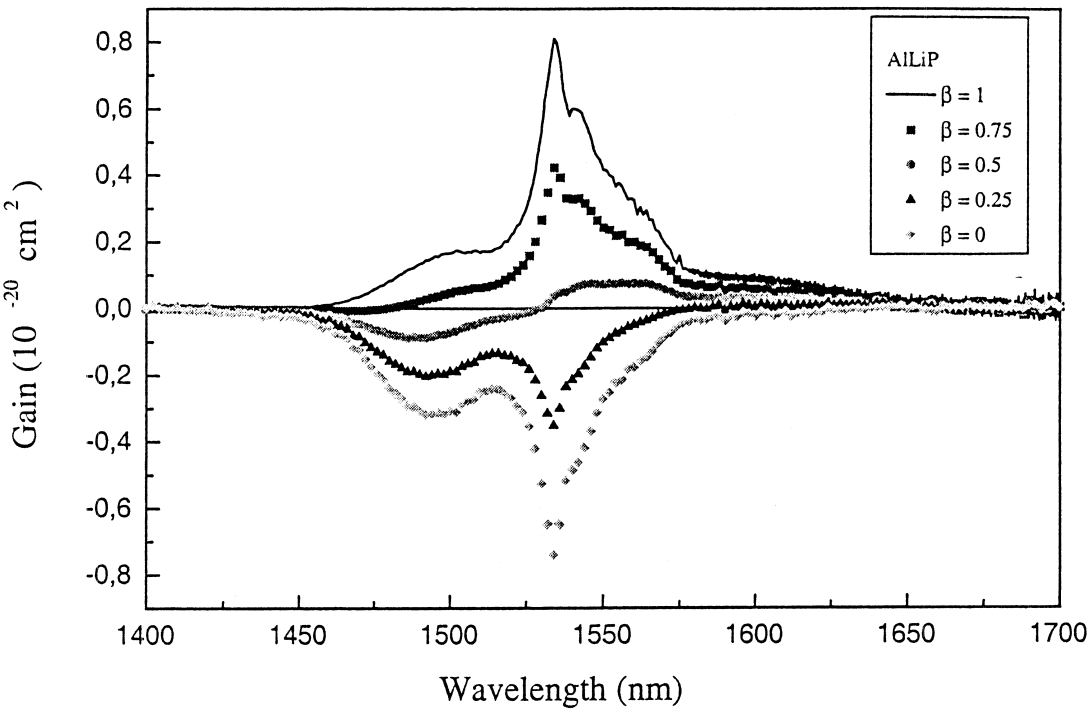

Fig. 9. The σ_g gain cross-section in the eye-safe range of the Er^{3+} ion in AlLiP phosphate glass.

strongest intensity zero-line of Yb^{3+} ion at 975 nm. Although materials were not optimised, laser output has been easily demonstrated with a 1-mm thickness sample and a 3% transmission mirror for Er^{3+} 1535 nm emission. The threshold is 97 mW and the laser efficiency is 19% for $LaLiP_4O_{12}$ compared to 21% for Kigre QX/Er in the

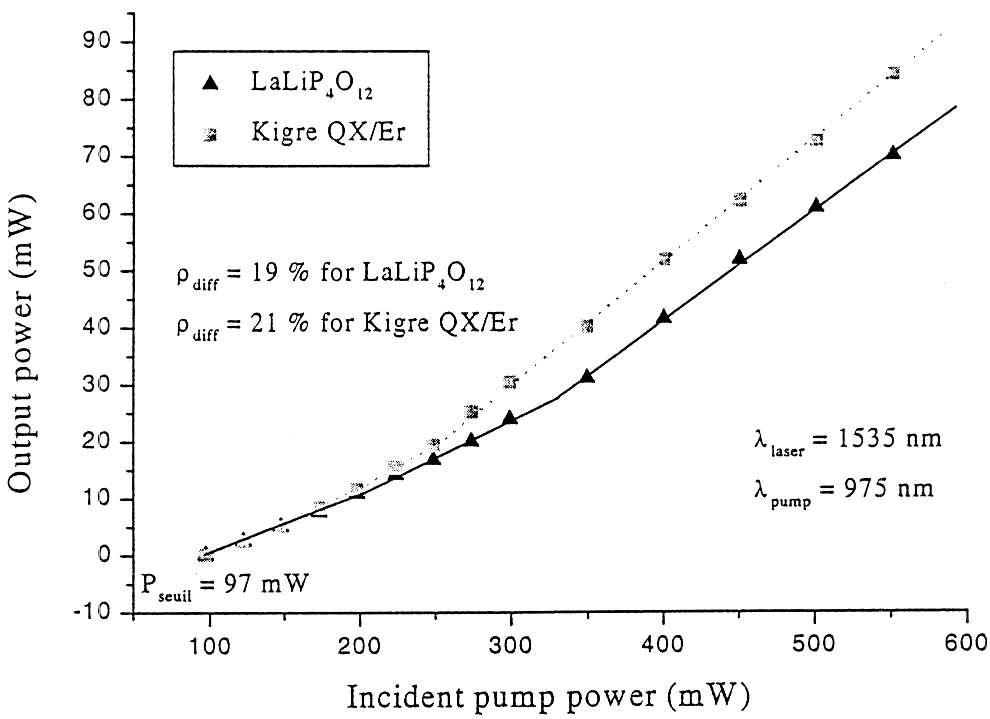

Fig. 10. Input–output characteristics of two laser phosphate glasses at room temperature.

250–600 mW input pump power (Fig. 10). Optimisations of both sizes of samples and activator concentrations are now needed to promote such new phosphate glasses.

4. Conclusion

The comparative study of Yb^{3+}–Er^{3+}-codoped phosphate glasses has allowed us to select the composition of Yb^{3+}–Er^{3+}-codoped $LaLiP_4O_{12}$ glass as a potential laser material. Of course, spectroscopic, laser and thermal properties need to be optimised for eye-safe laser source used at 1535 nm. Further work is in progress with the objective of characterizing short range order in phosphate glasses of different compositions and then to correlate physical properties with domains of the strongest cohesions in the nanostructure scale.

References

[1] A.F. Obaton, C. Labbé, P. Le Boulanger, B. Elouadi, G. Boulon, Spectrochem. Acta Part A 55 (1999) 263.

[2] A.F. Obaton, J. Bernard, C. Parent, G. le Flem, C. Labbé, P. Le Boulanger et al., Eur. Phys. J. 4 (1998) 315.

[3] A.F. Obaton, J. Bernard, C. Parent, G. Le Flem, J.M. Fernandez-Navarro, J.L. Adam et al., Advanced Solid-State Lasers, OSA, TOPS 26 (1999) 655.

[4] C. Parent, C. Lurin, F. Guillem, G. Le Flem, P. Hagenmuller, J. Phys. Chem. Solids 48 (1987) 207.